Journal of Leather Science and Engineering

RESEARCH Open Access

Wrapping collagen-based nanoparticle with macrophage membrane for treating multidrug-resistant bacterial infection

Yuanyuan Li[1], Jianming Xiong[1], Yi Hu[1], Wenjun Miao[1,2*] and He Huang[3*]

Abstract

Nowadays, multidrug-resistant (MDR) bacterial infectious diseases has become a thorny issue in the healthcare field. Owning to its intrinsic merits, photodynamic therapy (PDT) shows tremendous strengths in fighting against MDR bacterial infections. However, most photodynamic nanoplatforms exhibit unsatisfactory targeting efficiency towards bacteria and infection site, which may compromise the bactericidal effect of PDT. Herein, we firstly reported a bacteria-targeted collagen-based nanoparticle, named Ce6/Col/MM, for treating methicillin-resistant *Staphylococcus aureus* (MRSA)-infected wound. Ce6/Col/MM was fabricated by wrapping chlorin e6 (Ce6)-loaded collagen-based nanoparticles with macrophage membrane (MM), showing excellent photodynamic activity and good biocompatibility. In vitro studies demonstrated that Ce6/Col/MM could target to bacteria and then exhibit prominent antibacterial capacity against planktonic MRSA under light irradiation. Furthermore, the treatment of MRSA-infected wound in mice with Ce6/Col/MM plus light illumination resulted in potent bacterial inactivation and accelerated wound healing, accompanied by favorable histological compatibility. Collectively, Ce6/Col/MM with superior targeting ability towards bacteria, effective photodynamic antibacterial potency and minimal safety concerns, might be a powerful bactericidal nanoagent for treating infections caused by MDR bacteria.

Keywords: Collagen, Multidrug-resistant bacterial infections, Macrophage membrane, Photodynamic bactericidal therapy, Wound healing

*Correspondence: miaowj@njtech.edu.cn; huangh@njnu.edu.cn

[1] School of Pharmaceutical Sciences, Nanjing Tech University, Nanjing 211816, People's Republic of China
[3] School of Food Science and Pharmaceutical Engineering, Nanjing Normal University, Nanjing 210023, People's Republic of China
Full list of author information is available at the end of the article

Graphical Abstract

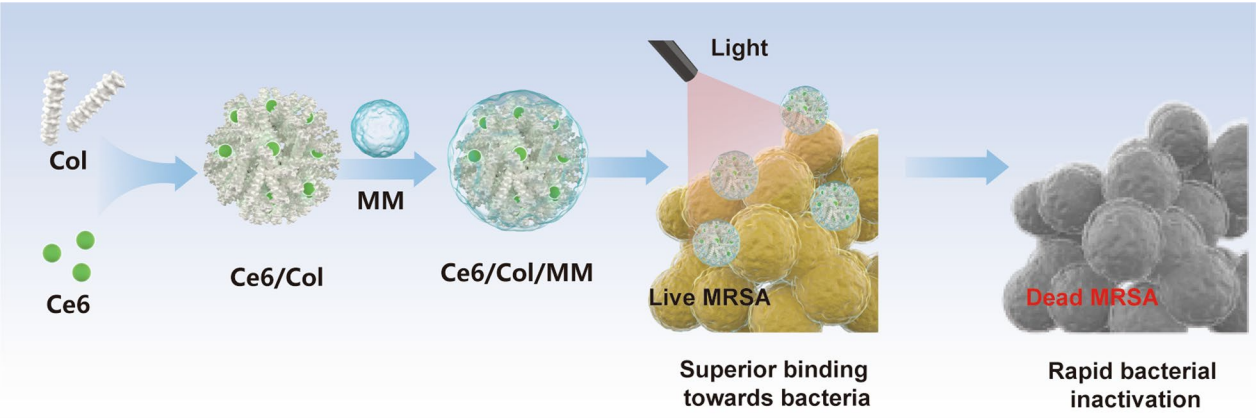

1 Introduction

Infectious diseases induced by multidrug-resistant bacteria, presenting a high rate of mortality and morbidity globally, contribute to more than 700,000 deaths worldwide every year and has become a severe threat to public health [1–3]. Nowadays, a broad range of antibiotics has been selected as first-in-class management to fight against the thorny problem in clinic. Unfortunately, the therapeutic effect of antibiotic therapy has been declining year by year, accompanied by rapid mutation of drug-resistant pathogens and recurrence of infection [4, 5]. Under the shadow of post-antibiotic era, photodynamic therapy (PDT) is a promising manner for treating MDR bacterial infections, which has attracted tremendous attention. Compared to antibiotic therapy, PDT exhibits a multitude of notable superiorities like broad-spectrum antibacterial activity, repeatable treatment, and negligible development of resistance [6–8]. To date, various kinds of photodynamic antibacterial nanosystems have been explored for MDR bacterial infections treatment. However, most of these proposal naonosystems showed low targeting efficiency to bacteria and poor accumulation in infection site due to lacking of specific-binding ability, resulting in discounted bactericidal effect and uncertain systematic toxicity [9, 10]. Thus, it would be of significance to construct bacteria-targeted photodynamic antibacterial nanoplatforms to overcome above issues.

Collagen, a vital structural protein, constitutes approximate 25–35% of total protein in human body and abundantly exists in fibrous tissue including bones, tendons, muscles and skin [11–13]. With satisfactory characteristic properties like good biodegradability, excellent biocompatibility and low immunogenicity, collagen often serves as a versatile carrier to deliver various kinds of drugs (gene, protein and growth factors) for diagnosis and therapy of diseases [14–16]. For instance, Mu's group has constructed collagen-based nanocomposite encapsulating silver nanoparticles (AgNP@collagen), exhibiting good blood compatibility, cytocompatibility and potent bacterial killing potency for treatment of *Pseudomonas aeruginosa*-infected mice [15]. Further, Thapa and co-workers demonstrated that collagen nanoplatform for sustained release of vancomycin could inhibit bacteria growth and accelerate recovery of MRSA-infected wound in vivo with negligible safety concerns [16]. Therefore, it is reasonable to speculate that collagen is an ideal cargo with minimal toxicity for effective delivery of bactericidal photosensitizers.

For pathogenic microorganism targeting, antibacterial agents decorated with cationic groups, peptides, antibodies and cell membranes has been explored [17–20]. In particular, macrophage, a laborious phagocytic cell, is responsible for eliminating pathogen and fighting against bacterial infections, which can recognize pathogen-associated molecular patterns through pattern-recognition receptors (PRR) to efficiently remove pathogens [21]. The membranes derived from macrophage are able to inherit PRR (mannan receptor [22], Toll like receptor [23], Scavenger receptor [24]) to recognize bacteria. For instance, Li and co-workers reported that macrophage membrane-coated antibacterial nanocomposite could rapidly recognize and kill drug-resistant bacteria in vitro [25]. Therefore, decorating of macrophage membrane on the surface of collagen-based antibacterial nanoagents is considered to be a promising strategy to provide potent binding ability to pathogenic microorganisms.

In this study, a photosensitizer, chlorin e6 (Ce6), was loaded into collagen-based nanoparticle (Col) via

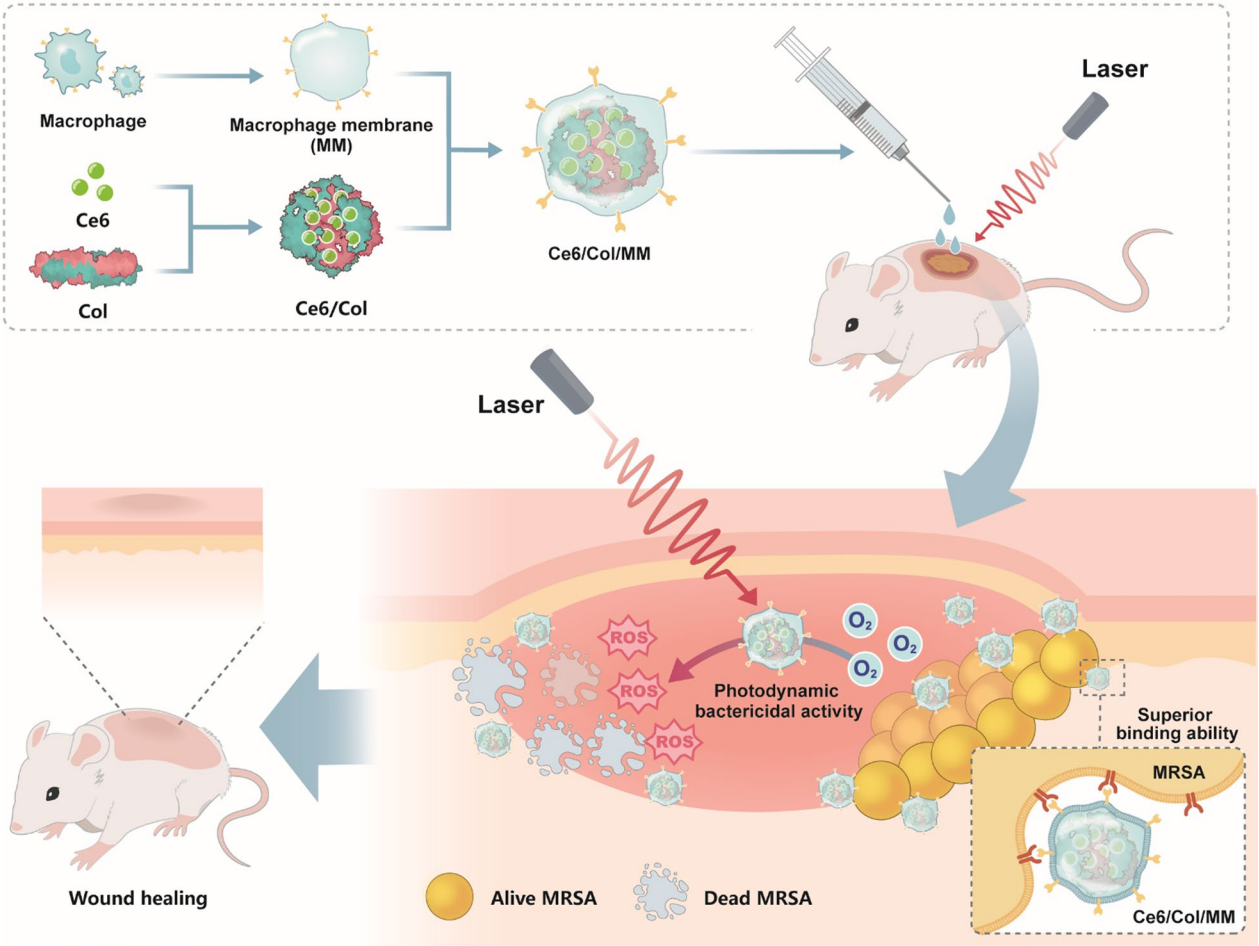

Scheme 1 Schematic illustration of a bacteria-targeted collagen-based nanoparticle, Ce6/Col/MM, for effective bacteria binding, enhanced bacteria killing and accelerated wound healing under light illumination

glutaraldehyde cross-linking, followed by wrapping with macrophage membrane (MM), which can enhance the biocompatibility of Ce6, as well as endow specific binding ability toward MDR bacteria. The resulting bacteria-targeted collagen-based nanoparticles, named Ce6/Col/MM, were expected to fight against MDR bacterial infection. We anticipate that the proposed nanoagents could specifically associate with bacteria by PRR, effectively kill bacteria under light irradiation via PDT and speed up the recovery of the MDR bacteria-infected wound in vivo (Scheme 1).

2 Experimental section

2.1 Materials

Ce6 was obtained from Frontier Scientific Inc. (West Logan, UT, USA). Col and 1,3-diphenylisobenzofuran (DPBF) were supplied by Sigma-Aldrich (St. Louis, USA). 3-(4,5-dimethyl-2-thiazolyl)-2,5-diphenyl-2H-tetrazolium bromide (MTT) and bicinchoninic acid (BCA) test kit were purchased from Beyotime Biotechnology Ltd. (Shanghai, China). Cyclophosphamide was purchased from Yuanye Biotechnology (Shanghai, China). Dulbecco's modified eagle medium (DMEM), Minimum essential medium (MEM), fetal bovine serum (FBS), protease inhibitor and 96-well plates were purchased from Thermo & Fisher Scientific Co. Ltd. (CA, USA). Distilled water (DW) with a resistivity higher than 18 MΩ cm^{-1} used in the experiments was made using Milli-Q Direct 16 Water Purification System (Millipore Corporation, Bedford, MA, United States). Other chemicals were supplied by Sinopharm Chemical Reagent Co., Ltd., China, and used as received.

Methicillin-resistant *Staphylococcus aureus* (MRSA) was kindly supplied by Dr. Yishan Zheng at The Second Hospital of Nanjing. Mouse macrophage (Raw 264.7) and fibroblasts (L929) cells were purchased from the Institute of Biochemistry and Cell Biology (Chinese Academy of Sciences, Shanghai, China). Raw264.7 and L929 cells

were cultured in DMEM and MEM medium, respectively, and maintained at 37 °C in a humidified atmosphere containing 5% CO_2. All media were supplemented with FBS (10%, v/v), penicillin (100 U mL^{-1}) and streptomycin (100 μg mL^{-1}), respectively.

2.2 Isolation of MM

MM were isolated using a hypotonic lysis approach with slight modifications [24]. In brief, Raw 264.7 cells were harvested using a cell scraper and resuspended in phosphate-buffered saline (PBS, pH 7.4) containing protease inhibitor (2 mM). The cell resuspension was sonicated with a tip for 3×60 s in ice and then centrifuged at $2000 \times g$ at 4 °C for 30 min. The precipitated MM was collected and washed with cold PBS and stored at − 80 °C for further use. The proteins of MM were determined by SDS-PAGE and quantified using the BCA kit.

2.3 Preparation of Ce6/Col/MM

Ce6/Col was prepared by glutaraldehyde cross-linking of collagen [26]. In brief, Ce6 (10 mg mL^{-1} in DMSO) was added into collagen aqueous solution (100 mg mL^{-1}) and stirred in dark for 2 h, and then ethanol was dropwise added to form Ce6/Col nanoparticle. For cross-linking, 4% glutaraldehyde (30 μL) was added into the above suspension and stirred for another 2 h at room temperature. The ethanol, glutaraldehyde and excess of free Ce6 were removed by dialysis to obtain the purified Ce6/Col nanosuspension.

For the preparation of Ce6/Col/MM, MM isolated from a total of 2×10^7 cells was mixed with Ce6/Col and sonicated with bath sonicator at a power of 100 W for 30 min. The surface-coated nanoparticles were centrifugated at $10{,}000 \times g$ for 30 min and washed with cold DW. And the purified Ce6/Col/MM were re-suspended in DW at the desired concentration and then stored at 4 °C.

2.4 Characterizations

The visible spectra of Ce6, Ce6/Col and Ce6/Col/MM (8 μg mL^{-1} of Ce6 equally) were recorded via microplate spectrophotometer (Multiskan™ GO, Thermo Fisher Scientific, United States). A fluorescence spectrophotometer (F-4500, HITACHI, Japan) was used to measure the fluorescence spectra. The emission spectra of nanoparticles were acquired from 450 to 850 nm when excited by 400 nm. Morphologies of Ce6/Col and Ce6/Col/MM were observed using transmission electron microscope (TEM, JEM-2100F, JELO, Japan). The immunogold labeling was introduced to verify the presence of MM in Ce6/Col/MM based on their surface protein CD14. Hydrodynamic diameters were determined by dynamic light scattering with a 10 mW He–Ne laser at 25 °C, and zeta potential values were determined by laser doppler microelectrophoresis at an angle of 22° using a Nano ZS90 Zetasizer (Malvern Instruments, the United Kingdom). The content of Ce6 in Ce6/Col/MM was calculated by absorbance at 650 nm based on the established calibration curve.

2.5 Light-triggered singlet oxygen generation

1,3-diphenylisobenzofuran (DPBF) was employed as $^1O_2$ trapping agent to assess light-trigger singlet oxygen ($^1O_2$) generation of Ce6/Col/MM [8]. In short, Ce6, Ce6/Col and Ce6/Col/MM (1.5 μg mL^{-1}, in term of Ce6) were irradiated using 660 nm laser (0.1 W cm^{-2}, 3 min) and the generated $^1O_2$ was captured by DPBF, leading to its absorption reduction at 410 nm. The absorption spectra of samples during irradiation were acquired at predetermined time points using microplate spectrophotometer. DMF containing DPBF alone were used as control.

2.6 Hemolysis assay

The hemolytic behavior of the Ce6/Col/MM was explored using mouse blood cells (RBCs) according to a standard protocol [27]. RBCs were isolated, purified and collected from the whole blood by centrifugation and washed with cold PBS. The 2% diluted RBCs suspension was mixed with serial concentrations of Ce6/Col/MM and incubated at 37 °C for 1 h. Then all samples were centrifuged ($100 \times g$, 15 min) and the absorbance of the supernatant at 541 nm was detected by microplate spectrophotometer. Saline and DW were used as negative and positive control, respectively.

2.7 Cytotoxicity study

The cytotoxicity of Ce6/Col/MM towards Raw 264.7 and L929 was evaluated by MTT assay [28]. Briefly, cells were seeded into 96-well plates at a density of 1×10^4 cells per well. In the following day, cells were treated with Ce6/Col/MM at various concentrations for 12 h in dark, and 10 μL of MTT (5 mg mL^{-1}) was added and incubated for another 4 h. After that, the medium was replaced with 150 μL dimethyl sulfoxide to dissolve formazan and the absorbance of each sample was recorded at 570 nm. The data were expressed as a percentage of the cell viability measure in the PBS groups. All groups were assessed at least in sextuplicate.

2.8 Targeting ability evaluation

The targeting ability of Ce6/Col/MM towards bacteria was assessed by flow cytometry. In short, 900 μL of MRSA suspension (1×10^8 CFU mL^{-1}) was incubated with free Ce6, Ce6/Col or Ce6/Col/MM at 37 °C for 1 h

in dark. After that, bacteria were collected by centrifugation and analyzed using a NovoCyte 2060R flow cytometer and ACEA NovoExpress software (ACEA Biosciences Inc., San Diego, CA).

2.9 Photodynamic antibacterial activity in vitro

The bactericidal activity of Ce6/Col/MM against MRSA was quantitatively assessed by the standard plate counting method [29]. In detail, 900 μL of bacteria suspension (1×10^8 CFU mL^{-1}) was mixed with free Ce6, Ce6/Col, MM or Ce6/Col/MM in dark, respectively. After incubated at 37 °C for 30 min, all samples were exposed to 660 nm light at an intensity of 100 mW cm^{-2} for 3 min or in dark. The colony-forming units (CFU) were counted by inoculating 100 μL of bacteria suspension onto LB agar plate and growing at 37 °C for 24 h.

2.10 In vivo antibacterial effect study

To evaluate the antibacterial efficacy in vivo, the MRSA-infected wound model was established. In detail, cyclophosphamide (150 mg kg^{-1}) was intraperitoneally injected to the mice for 4 days to create a temporary state of neutropenia. Afterward, mice were slashed into a circular wound of 5 mm diameter and injected with 50 μL of MRSA (10^7 CFU mL^{-1}) to construct the infected wound model. Mice with wound were randomly grouped (a) PBS + Light, (b) Ce6/Col/MM, (c) free Ce6 + Light, (d) Ce6/Col + Light and (e) Ce6/Col/MM + Light (0.4 mg kg^{-1} of Ce6) (n = 6). The mice were exposed to 660 nm laser (1.2 W cm^{-2}) for 10 min at 4 h post-administration or in dark. At day 2 after treatment, aliquots of diluted exudate from wound were spread on LB agar, where the grown colonies were counted for analysis. Moreover, the skin tissue of the infected wound region of mice was collected and ground. Then the collagenase level generated by MRSA of each sample was determined by ELISA kit at day 2 and 7 after various treatments. The area of wound was measured and photographed every two days. For histological analysis, the wound tissues of mice were collected and stored in 4% paraformaldehyde for further Masson staining at day 14 post-treatment.

To evaluate the safety profile in vivo, the body weight of mice subjected to various treatments was recorded throughout the experimental period and the major organs (heart, liver, spleen, lung and kidney) of mice were collected and sectioned for hematoxylin and eosin (H&E) staining.

2.11 Statistics

All statistical analyses were performed using GraphPad Prism (version 8.0, GraphPad Ltd., China). ANOVA was used to analyze all data with a Student–Newman–Keuls test for post-hoc pairwise comparisons.

3 Results and discussion

3.1 Preparation and characterizations

Ce6/Col/MM was fabricated by loading of Ce6 into collagen nanoparticle and then wrapping with MM. As depicted in Fig. 1a, no obvious absorption of MM was observed at visible range. In contrast, Ce6/Col/MM had two characteristic bands at 400 and 660 nm, originating from Ce6 chromophore, demonstrating the successful encapsulation of Ce6. The average drug loading and encapsulation efficiency of Ce6 were 1.5% and 83.3%, respectively. Compared to free Ce6, Ce6/Col/MM exhibited an intense and narrow fluorescence emission at 660 nm, mainly attributing to stabilizing ability of nanoparticles toward photosensitizer in aqueous conditions (Fig. 1b). Immunoelectron microscopy following anti-CD14 gold staining proved the successful decorating with MM on the surface of Ce6/Col/MM (Additional file 1: Fig. S1). SDS-PAGE analysis (Fig. 1c) showed that the composition of membrane proteins of MM in Ce6/Col/MM was well preserved during the preparation. The average hydrodynamic size of MM and Ce6/Col was 156.4 ± 6.5 and 128.3 ± 6.5 nm, respectively (Fig. 1d). After decorated with MM, the size of Ce6/Col/MM was increased to 141.6 + 7.1 nm, implying that the thickness of MM was around 6 nm, which was well consistent with previous reports [30, 31]. TEM image (Fig. 1e & Additional file 1: Fig. S2) showed that Ce6/Col/MM was spherical with the core–shell structure compared to spherical Ce6/Col, and their size were relatively smaller than that from DLS measurement due to shrinking of nanoparticles in vacuum. In addition, the wrapping of MM resulted in a decrease in the zeta potential of Ce6/Col from − 10.9 to − 25.6 mV, which is similar to that of MM (Fig. 1f). Collectively, macrophage membrane-coated collagen-based nanoparticles, Ce6/Col/MM, were successfully constructed.

3.2 Photodynamic activity of Ce6/Col/MM

We then assessed the photodynamic ability of Ce6/Col/MM in response to light irradiation using DPBF as a molecule probe. As shown in Fig. 2a–c, the absorbance of DPBF in free Ce6, Ce6/Col and Ce6/Col/MM groups sharply was decayed and the DPBF-consuming rate of Ce6/Col and Ce6/Col/MM resembled to that of free Ce6 under irradiation, implying their similar $^1O_2$ generation capacity. Upon irradiation for 90 and 150 s, the percentage of $^1O_2$ in Ce6/Col/MM group reached by 45.2% and 90.3%, respectively, versus 43.1% and 90.6% in case of free Ce6, respectively (Fig. 2d). These results suggested that the loading of Ce6 into MM-coated collagen nanoparticles could scarcely affect the photosensitizing potential of Ce6.

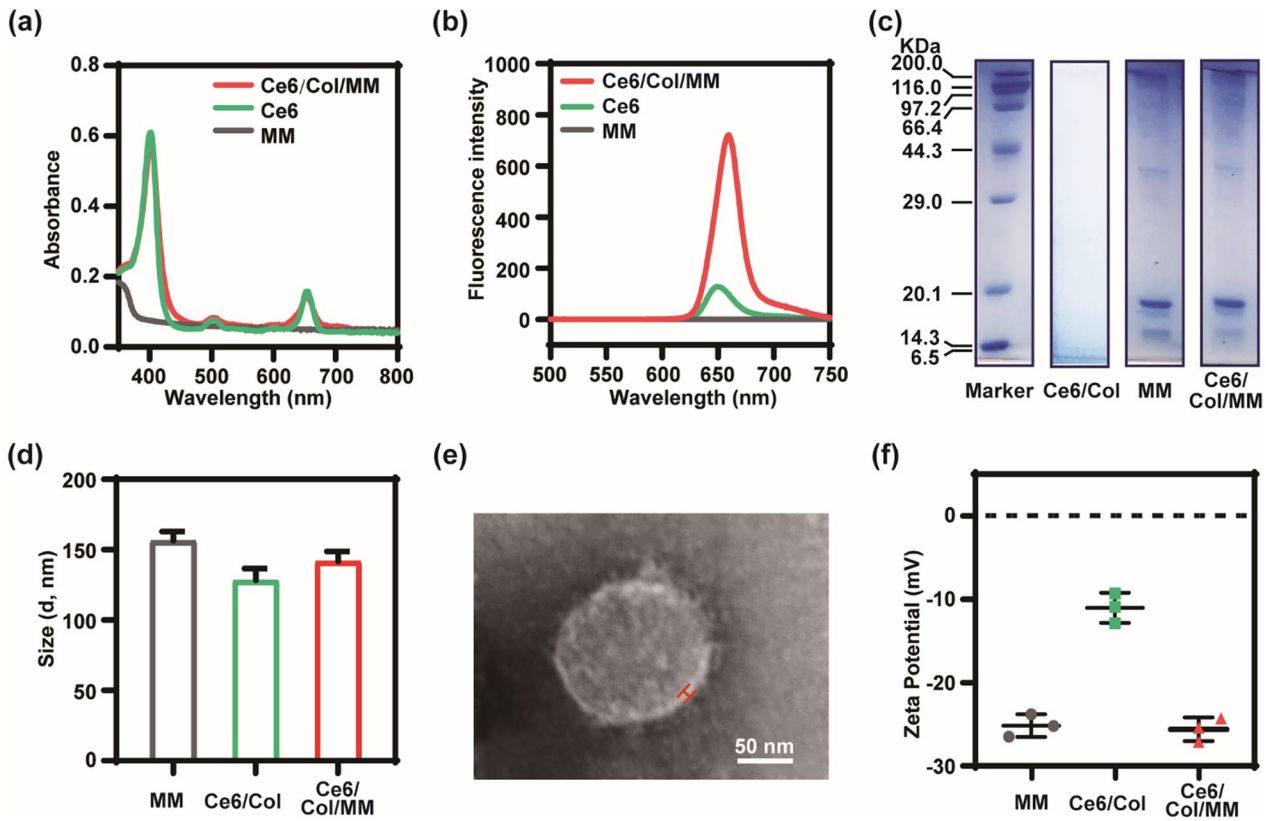

Fig. 1 Characterizations of Ce6/Col/MM. **a** Visible and **b** fluorescence spectra of MM, Ce6 (8 μg mL^{-1}) and Ce6/Col/MM (excited at 400 nm). **c** The protein composition of Ce6/Col, MM and Ce6/Col/MM by SDS-PAGE analysis. **d** Hydrodynamic diameter of MM, Ce6/Col and Ce6/Col/MM. **e** TEM image of Ce6/Col/MM, red line indicated the thickness of MM on the surface of Ce6/Col/MM. **f** Plot showing the zeta potentials of MM, Ce6/Col and Ce6/Col/MM. Data are shown as mean ± S.D. (n = 3)

3.3 Light-induced antibacterial activity in vitro

We first investigated the targeting ability of Ce6/Col/MM towards bacteria via flow cytometer. Compared with PBS, Ce6 and Ce6/Col were moderately absorbed by MRSA, and there was no obvious difference between them. However, Ce6/Col/MM showed enhanced association efficacy toward bacteria under identical experimental conditions (Fig. 3a). The fluorescence intensity of Ce6/Col/MM-treated bacteria was 5.7 and 4.9 folds higher than those treated with Ce6 and Ce6/Col, respectively (Fig. 3b). The superior association potency of Ce6/Col/MM with bacteria was favorable for improved photodynamic bactericidal effect in response to light irradiation. In absence of illumination, the survival rate of MRSA in all group remained nearly 100%, even the concentration was up to 2.0 μg mL^{-1} (in terms of Ce6), suggesting no antibacterial effect of collagen-based nanoparticles in dark. We also found that MM exhibited negligible bactericidal activity towards MRSA under illumination (Additional file 1: Fig. S3). When MRSA was treated with free Ce6, Ce6/Col or Ce6/Col/MM and exposed to light irradiation, their viability was gradually decreased and inversely proportional to the concentration of Ce6 (Fig. 3a–c). The reduction of log unit in Ce6/Col group + light was averagely 2.0 and 3.7 at 1.0 and 2.0 μg mL^{-1} of Ce6, respectively, ascribing to the photodynamic bacterial killing ability of Ce6-based antimicrobial agents. By contrast, Ce6/Col/MM exhibited conspicuous bactericidal effect in response to illumination. The log units dropped to 1.8 at 2.0 μg mL^{-1} of Ce6, which was much lower than that of free Ce6 or Ce6/Col. This phenomenon could be partially explained by Ce6/Col/MM might efficiently anchor to bacteria and trigger potent photodynamic bactericidal performance as irradiation proceeded [25]. These results justified the excellent bacteria inactivation effect of Ce6/Col/MM against MRSA via photodynamic bactericidal therapy.

3.4 In vitro biocompatibility assay

Good biocompatibility is the premise for exploring the nanoparticles as a light-triggered bactericidal agent. We next assessed the cytotoxicity of Ce6/Col/MM against

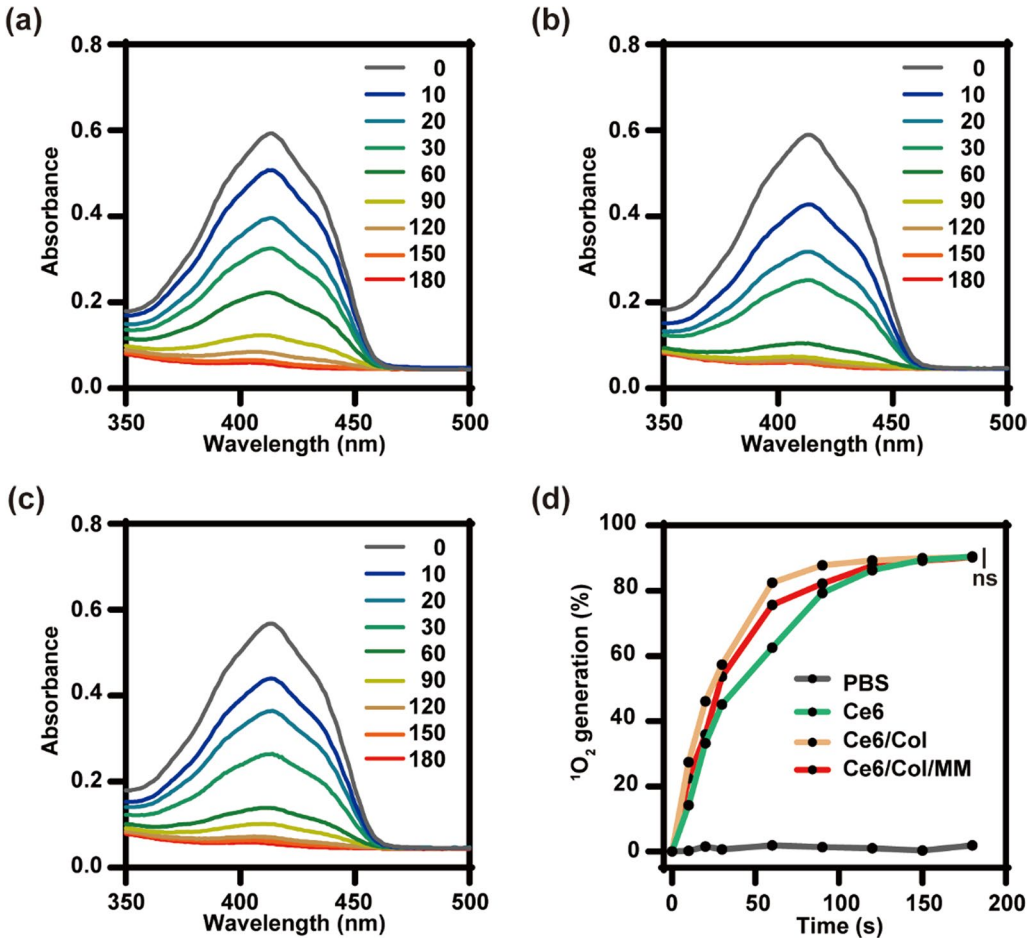

Fig. 2 Photodynamic activity of Ce6/Col/MM. **a** Ce6, **b** Ce6/Col or **c** Ce6/Col/MM containing DPBF, $^1O_2$ trapping agent, was irradiated with 660 nm and the absorbance reduction of DPBF at 410 nm indicates the generation of singlet oxygen. **d** Singlet oxygen generation percentages of Ce6, Ce6/Col and Ce6/Col/MM at predetermined time points based on (**a**)–(**c**). ns: no significant difference compared to free Ce6 and Ce6/Col

Raw 264.7 and L929 cells, representing immune and tissue cells, respectively, via MTT assay. After treatment for 24 h in dark, negligible toxicity of Ce6/Col/MM was observed in both cell lines. When its concentration reached to 50 μg mL^{-1} (in terms of Ce6), over 90% of viability was remained regardless of cell type, suggesting the satisfactory cytocompatibility of Ce6/Col/MM (Fig. 4a, b). Meanwhile, nanoparticles should be accepted by the host tissue without prompting any undesirable effect, such as lysing of erythrocytes [32]. The hemolysis study revealed that Ce6/Col/MM led to inappreciable hemolysis rate to rabbit blood cells (lower than 5%) even at the concentration up to 40 μg mL^{-1} (Fig. 4c). Collectively, these results demonstrated that Ce6/Col/MM have favorable safety profiles in vitro, broadening the possibilities for their further biomedical applications.

3.5 Light-triggered antibacterial activity and wound healing in vivo

We further established a MRSA-infected wound model in mice to evaluate the photodynamic antibacterial performance and wound healing effect of Ce6/Col/MM. The experimental procedure was shown in Fig. 5a. For exploration of bactericidal ability, the wound exudate was collected and the CFU of MRSA was quantified on day 2 post-treatment. As depicted in Fig. 5b, c, the number of bacteria in Ce6 and Ce6/Col group was partially decreased compared to PBS group under light illumination and the survival percentage of bacteria was 67.4 ± 6.1% and 59.8 ± 9.7%, respectively. These observations implied that neither Ce6 nor Ce6/Col plus light possessed satisfied antibacterial efficacy. Strikingly, the bacterial viability in Ce6/Col/MM + light group was

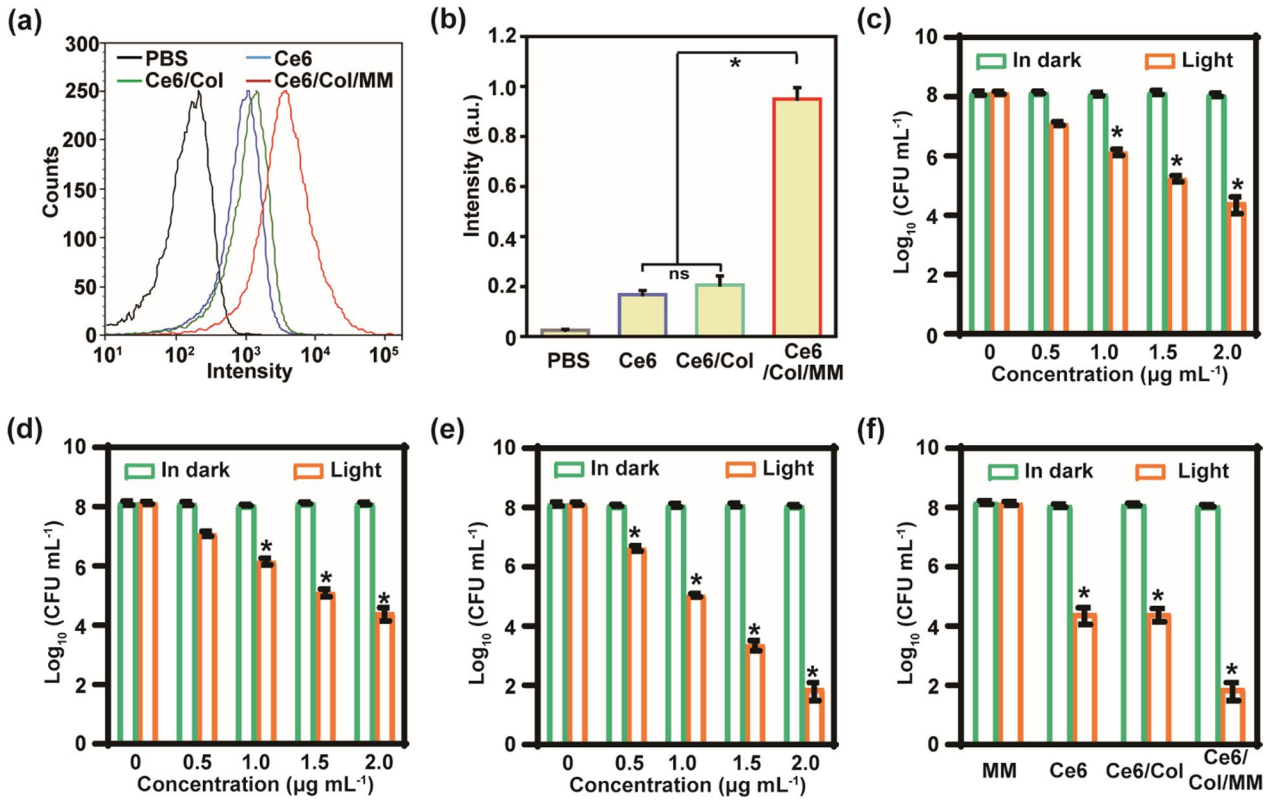

Fig. 3 In vitro enhanced antibacterial activity of Ce6/Col/MM. **a** Flow cytometry analysis of MRSA subjected to Ce6, Ce6/Col or Ce6/Col/MM (10 μg mL^{-1}) treatment for 1 h. **b** quantitative analysis of fluorescence intensity based on (**a**). Log value of survived MRSA treated with free Ce6 (**c**), Ce6/Col (**d**) or Ce6/Col/MM (**e**) at serial concentrations and irradiated with 660 nm light (100 mW cm^{-2}, 3 min), compared among groups (**f**) at 2.0 μg mL^{-1} of Ce6. Data are shown as means ± S.D. ($n \geq 3$). *$p < 0.005$

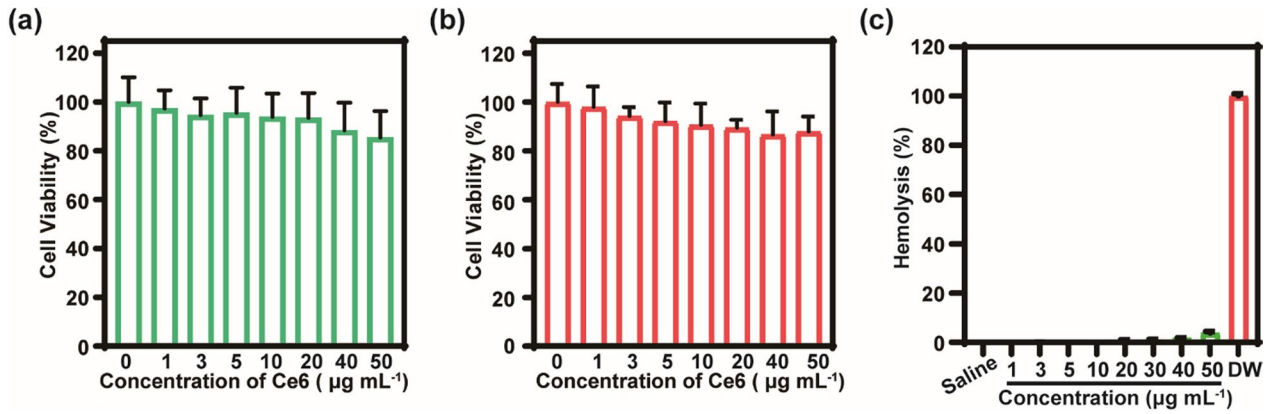

Fig. 4 In vitro biocompatibility of Ce6/Col/MM. The viability of Raw 264.7 (**a**) and L929 (**b**) cells treated with Ce6/Col/MM at various concentrations in dark for 24 h using MTT assay. **c** Hemolysis rate of RBC subjected to Ce6/Col/MM treatment at 37 °C for 1 h. Data are shown as mean ± S.D. ($n \geq 3$)

reduced to 6.7 ± 0.6%, much lower than those in other groups, exhibiting most potent bacteria inactivation effect of Ce6/Col/MM with light irradiation. At day 2 post-treatment, we found that the bacterial collagenase level in Ce6/Col/MM, Ce6/Col + light and Ce6/Col/MM + light group was signifcantly lower than that in PBS + light group, which can be ascribed to the neutralization potency of collagen-based nanoparticles.

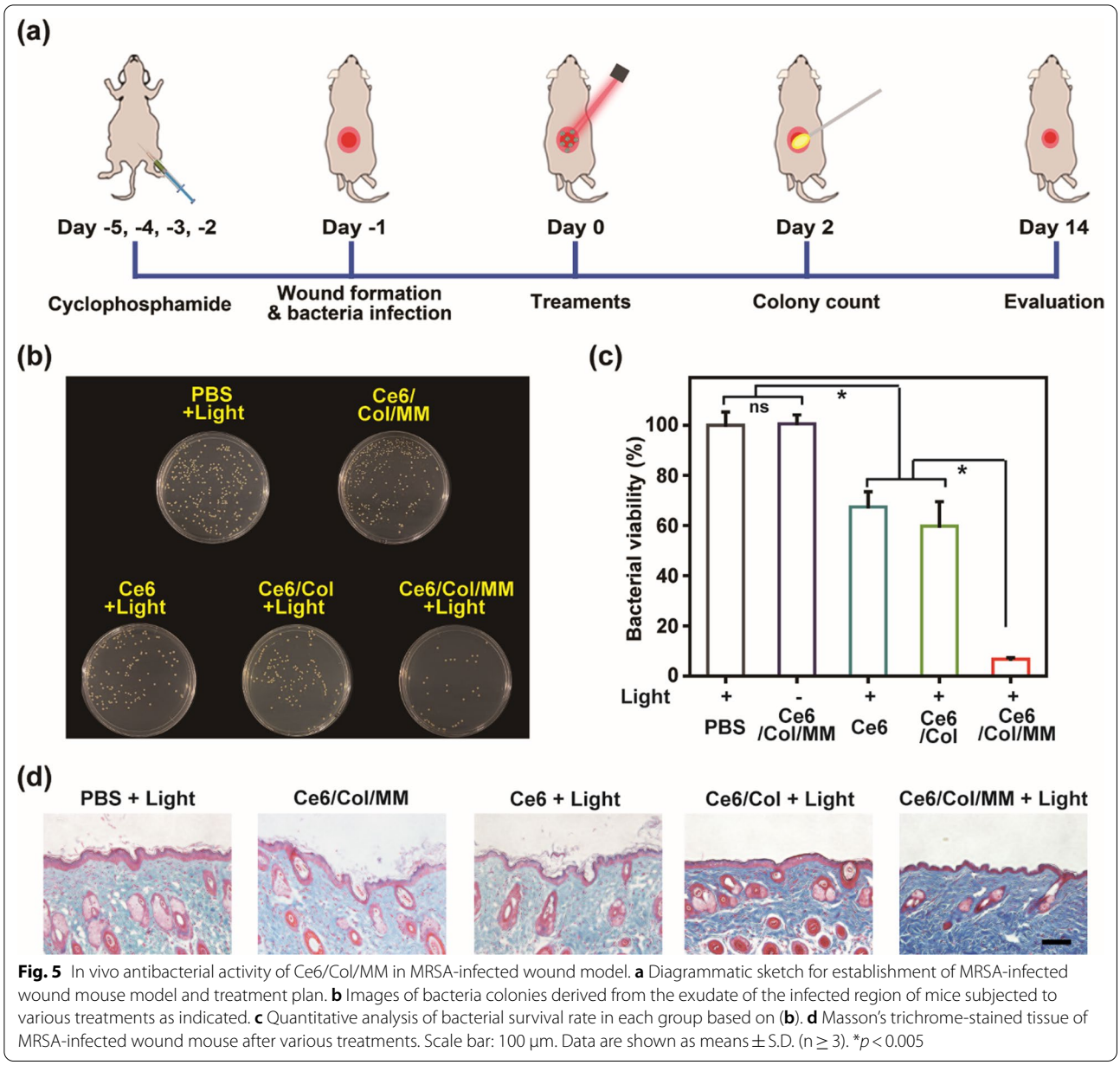

Fig. 5 In vivo antibacterial activity of Ce6/Col/MM in MRSA-infected wound model. **a** Diagrammatic sketch for establishment of MRSA-infected wound mouse model and treatment plan. **b** Images of bacteria colonies derived from the exudate of the infected region of mice subjected to various treatments as indicated. **c** Quantitative analysis of bacterial survival rate in each group based on (**b**). **d** Masson's trichrome-stained tissue of MRSA-infected wound mouse after various treatments. Scale bar: 100 μm. Data are shown as means ± S.D. ($n \geq 3$). *$p < 0.005$

Moreover, the bacterial collagenase content of infected tissue further remained unchanged at day 7 in Ce6/Col/MM + light group, in contrast to the highly elevated level of other groups (~ 30 ng/mg tissue (Additional file 1: Fig. S4). Furthermore, Masson's trichrome staining revealed that the skin tissue in infected wound in Ce6/Col/MM + light group displayed a darker blue than other groups at day 14 after corresponding treatment (Fig. 5d). These results suggested that Ce6/Col/MM not only displayed strongly bactericidal potential but also consumed collagenase produced by pathogenic microorganism in the infected sites, which could promote collagen fiber deposition over treatment course [33, 34].

As depicted in Fig. 6a, the wound healing process was monitored photographically throughout treatment period. Except Ce6/Col/MM with illumination group, the infected wound of mice received various treatments exhibited severe abscess, again proving efficient bactericidal ability of Ce6/Col/MM in infected mice. Furthermore, the treatment of Ce6/Col/MM + light facilitated a faster wound closure compared to those in other groups. The area of Ce6/Col/MM-treated wound had recovered by 90.6% and the wound was healed with new epidermal tissue after 14 days. While 62.1%, 65.7% and 56.9% of wound were observed in Ce6/Col/MM, Ce6 + light and Ce6/Col + light group, respectively (Fig. 6b). These

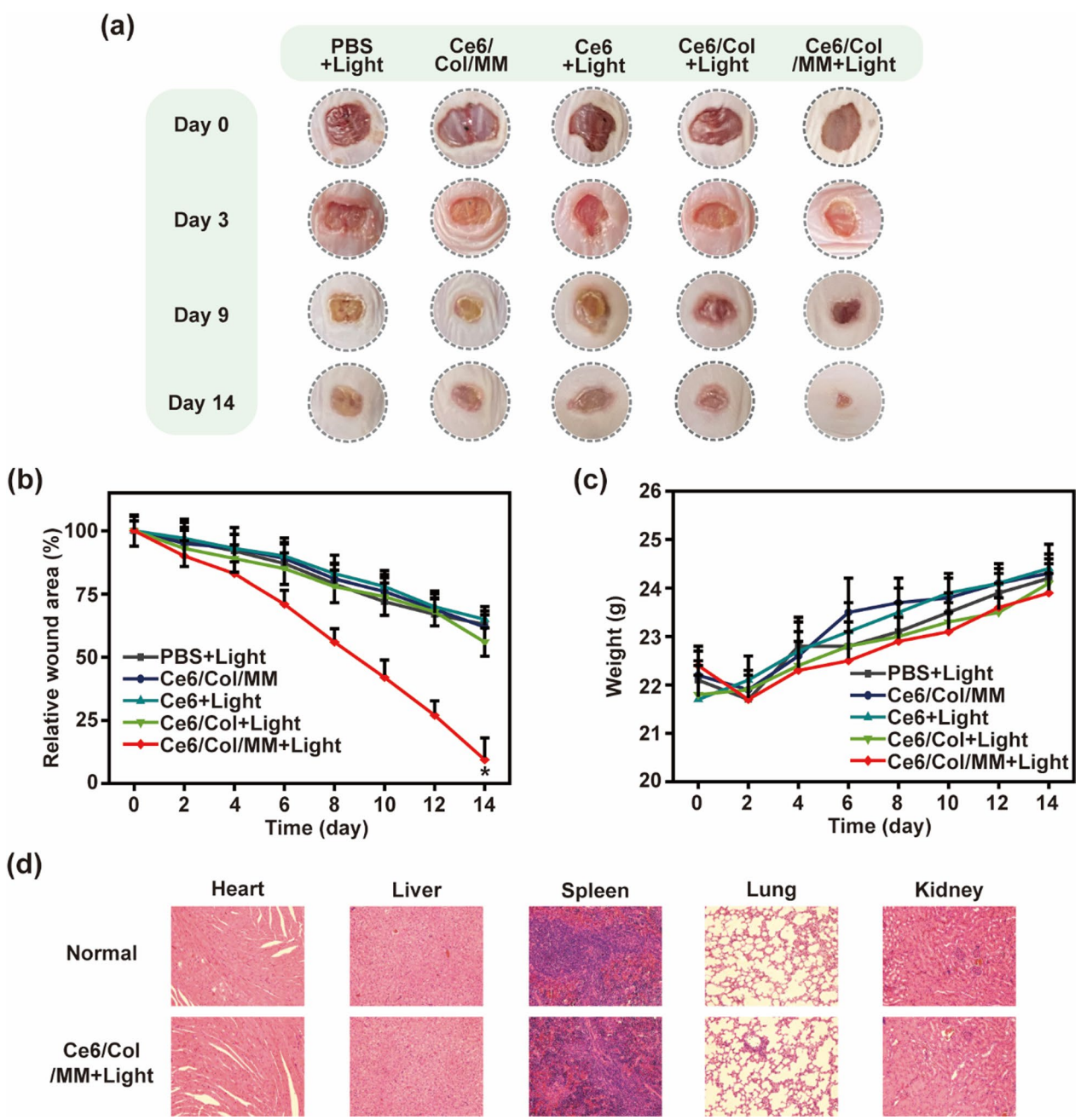

Fig. 6 Healing effect and histological biocompatibility of MRSA-infected wound mice received various treatments as indicated. **a** Photographs of wound region at predetermined time points. **b** Relative wound area and **c** body weight of mice with above mentioned treatments. **d** H&E-stained sections of major organs (heart, liver, spleen, lung and kidney) of Ce6/Col/MM-treated mice. Scale bar: 100 μm. Data are shown as means ± S.D. (n = 6). *$p < 0.005$ compared to the Ce6 + Light group

results demonstrated that Ce6/Col/MM could accelerate regeneration of skin tissue and wound healing. In addition, the weight of mice in all groups had been negligibly affected throughout treatment period (Fig. 6c); compare to normal group, histological analysis of major organs revealed no obvious inflammation or damage (Fig. 6d), confirming the biocompatibility of collagen-based nanoparticle. Thus, Ce6/Col/MM could be a safe antibacterial agent for combating infection caused by drug-resistant bacteria and promoting wound healing.

4 Conclusion

In summary, we have firstly fabricated bacteria-targeting collagen-based nanoparticles, Ce6/Col/MM, in fight against MDR bacteria-infected wound via photodynamic antibacterial therapy. It exhibited negligible cytotoxicity, favorable optical properties and efficient singlet oxygen generation capacity. With the aid of MM, Ce6/Col/MM could easily associate with pathogenic microorganism, leading to effective delivery of photosensitizer and enhanced photodynamic bactericidal efficacy against antibiotic-resistant bacteria, MRSA. In vivo experiment demonstrated that Ce6/Col/MM combining light irradiation showed notable bacterial inactivation ability, promoting collagen fiber deposition and wound healing in MRSA-infected mice. Additionally, minimal safety concern of Ce6/Col/MM was verified by histological analysis of major organs. Therefore, bacteria-targeting collagen-based nanoparticles exhibited acceptable biocompatibility, notable bactericidal ability, as well as accelerated wound healing, providing a promising antibacterial nanoagent for treating MDR bacterial infection.

Supplementary Information

The online version contains supplementary material available at https://doi.org/10.1186/s42825-022-00106-2.

Additional file 1: Fig. S1. Immunoelectron microscopy image of Ce6/Col/MM following anti-CD14 gold staining. **Fig. S2.** TEM image of Ce6/Col. **Fig. S3.** Log value of survived MRSA treated with MM at serial concentrations in dark or with irradiation (660 nm, 100 mW cm^{-2}, 3 min). **Fig. S4.** Quantitative analysis of bacterial collagenase level of the infected region of mice at day 2 and day 7 after various treatments. Data are shown as means ± S.D. ($n \geq 3$). *$p < 0.005$ compared to PBS plus light group.

Acknowledgements

This work was supported by research grants from the National Natural Science Foundation of China (No. 51603101).

Author contributions

WJM and HH designed this project and revised the manuscript. YYL performed experiments, analyzed data and wrote the manuscript. JMX performed experiments and draw the scheme. YH reviewed the manuscript. All authors read and approved the final manuscript.

Availability of data and materials

All data generated or analyzed during this study are included in this published article.

Declarations

Ethics approval and consent to participate

All animal experiments were conducted in compliance with the guidelines of the Administration Committee of Experimental Animals in Jiangsu Province and the Animal Care Committee of Nanjing Tech University (No. 20211202-03). Male Balb/c mice (25 ± 3 g) were purchased from Institute of Comparative Medicine, Yangzhou University.

Competing interests

The authors declare that they have no known competing financial interests or personal relationships that could have appeared to influence the work reported in this paper.

Author details

[1]School of Pharmaceutical Sciences, Nanjing Tech University, Nanjing 211816, People's Republic of China. [2]State Key Laboratory of Materials-Oriented Chemical Engineering, Nanjing Tech University, Nanjing 211816, People's Republic of China. [3]School of Food Science and Pharmaceutical Engineering, Nanjing Normal University, Nanjing 210023, People's Republic of China.

Received: 16 August 2022 Revised: 3 November 2022 Accepted: 8 November 2022
Published online: 02 December 2022

References

1. Crofts TS, Gasparrini AJ, Dantas G. Next-generation approaches to understand and combat the antibiotic resistome. Nat Rev Microbiol. 2017;15:422–34.
2. Aslam B, Wang W, Arshad MI, Khurshid M, Muzammil S, Rasool MH, Nisar MA, Alvi RF, Aslam MA, Qamar MU, Salamat MKF, Baloch Z. Antibiotic resistance: a rundown of a global crisis. Infect Drug Resist. 2018;11:1645–58.
3. Seiple IB, Zhang Z, Jakubec P, Langlois-Mercier A, Wright PM, Hog DT, Yabu K, Allu SR, Fukuzaki T, Carlsen PN, Kitamura Y, Zhou X, Condakes ML, Szczypiński FT, Green WD, Myers AG. A platform for the discovery of new macrolide antibiotics. Nature. 2016;533:338–45.
4. Foster TJ. Antibiotic resistance in *Staphylococcus aureus*. Current status and future prospects. FEMS Microbiol Rev. 2017;41:430–49.
5. Wong D, Nielsen TB, Bonomo RA, Pantapalangkoor P, Luna B, Spellberg B. Clinical and pathophysiological overview of acinetobacter infections: a century of challenges. Clin Microbiol Rev. 2017;30:409–47.
6. Zhang R, Li Y, Zhou M, Wang C, Feng P, Miao W, et al. Photodynamic chitosan nano-assembly as a potent alternative candidate for combating antibiotic-resistant bacteria. ACS Appl Mater Interfaces. 2019;11:26711–21.
7. Xiu W, Wan L, Yang K, Li X, Yuwen L, Dong H, Mou Y, Yang D, Wang L. Potentiating hypoxic microenvironment for antibiotic activation by photodynamic therapy to combat bacterial biofilm infections. Nat commun. 2022;13:3875.
8. Niu P, Dai J, Wang Z, Wang Y, Feng D, Li Y, Miao W. Sensitization of antibiotic-resistant gram-negative bacteria to photodynamic therapy via perfluorocarbon nanoemulsion. Pharmaceuticals. 2022;15:156.
9. Shao L, Pan Y, Hua B, Xu S, Yu G, Wang M, Liu B, Huang F. Constructing adaptive photosensitizers via supramolecular modification based on pillararene host-guest interactions. Angew Chem Int Ed. 2020;59:11779–83.
10. Wang Y, Wu W, Liu J, Manghnani PN, Hu F, Ma D, Teh C, Wang B, Liu B. Cancer-cell-activated photodynamic therapy assisted by Cu(II)-based metal–organic framework. ACS Nano. 2019;13:6879–90.
11. Mbese Z, Alven S, Aderibigbe BA. Collagen-based nanofibers for skin regeneration and wound dressing applications. Polymers. 2021;13:4368.
12. Han Y, Hu J, Sun G. Recent advances in skin collagen: functionality and non-medical applications. J Leather Sci Eng. 2021;3:1–12.
13. Zhang X, Xu S, Shen L, Li G. Factors affecting thermal stability of collagen from the aspects of extraction, processing and modification. J Leather Sci Eng. 2020;2:1–29.
14. Dorazilova J, Muchova J, Smerkova K, Kociova S, Divis P, Kopel P, Vesely R, Pavlinakova V, Adam V, Vojtova L. Synergistic effect of chitosan and selenium nanoparticles on biodegradation and antibacterial properties of collagenous scaffolds designed for infected burn wounds. Nanomaterials. 2020;10:1971.
15. Ge L, Xu Y, Li X, Yuan L, Tan H, Li D, Mu C. Fabrication of antibacterial collagen-based composite wound dressing. ACS Sustain Chem Eng. 2018;6:9153–66.
16. Thapa RK, Kiick KL, Sullivan MO. Encapsulation of collagen mimetic peptide-tethered vancomycin liposomes in collagen-based scaffolds for infection control in wounds. Acta Biomater. 2020;103:115–28.
17. Hu D, Li H, Wang B, Ye Z, Lei W, Jia F, Jin Q, Ren KF, Ji J. Surface-adaptive gold nanoparticles with effective adherence and enhanced photothermal ablation of methicillin-resistant *Staphylococcus aureus* biofilm. ACS Nano. 2017;11:9330–9.

18. Huang N, Chen X, Zhu X, Xu M, Liu J. Ruthenium complexes/polypeptide self-assembled nanoparticles for identification of bacterial infection and targeted antibacterial research. Biomaterials. 2017;141:296–313.
19. Brezden A, Mohamed MF, Nepal M, Harwood JS, Kuriakose J, Seleem MN, Chmielewski J. Dual targeting of intracellular pathogenic bacteria with a cleavable conjugate of kanamycin and an antibacterial cell-penetrating peptide. J Am Chem Soc. 2016;138:10945–9.
20. Zhang Y, Zhang J, Chen W, Angsantikul P, Spiekermann KA, Fang RH, Gao W, Zhang L. Erythrocyte membrane-coated nanogel for combinatorial antivirulence and responsive antimicrobial delivery against Staphylococcus aureus infection. J Control Release. 2017;263:185–91.
21. Li C, Wang Y, Li Y, Yu Q, Jin X, Wang X, Jia A, Hu Y, Han L, Wang J, Yang H, Yan D, Bi Y, Liu G. HIF1alpha-dependent glycolysis promotes macrophage functional activities in protecting against bacterial and fungal infection. Sci Rep. 2018;8:3603.
22. Thamphiwatana S, Angsantikul P, Escajadillo T, Zhang Q, Olson J, Luk BT, Zhang S, Fang RH, Gao W, Nizet V, Zhang L. Macrophage-like nanoparticles concurrently absorbing endotoxins and proinflammatory cytokines for sepsis management. PNAS. 2017;114:11488–93.
23. Kawai T, Akira S. The role of pattern-recognition receptors in innate immunity: update on Toll-like receptors. Nat Immunol. 2010;11:373–84.
24. Che J, Sun L, Shan J, Shi Y, Zhou Q, Zhao Y, Sun L. Artificial lipids and macrophage membranes coassembled biomimetic nanovesicles for antibacterial treatment. Small. 2022;18:2201280.
25. Li J, Wang Y, Yang J, Liu W. Bacteria activated-macrophage membrane-coated tough nanocomposite hydrogel with targeted photothermal antibacterial ability for infected wound healing. Chem Eng J. 2021;420:127638.
26. Cheng HB, Qiao B, Li H, Cao J, Luo Y, Kotraiah SKM, Zhao J, Wang Z, Lee JY, Liang XJ, Yoon J. Protein-activatable diarylethene monomer as a smart trigger of noninvasive control over reversible generation of singlet oxygen: a facile, switchable, theranostic strategy for photodynamic-immunotherapy. J Am Chem Soc. 2021;143:2413–22.
27. Li Y, Feng P, Wang C, Miao W, Huang H. Black phosphorus nanophototherapeutics with enhanced stability and safety for breast cancer treatment. Chem Eng J. 2020;400:125851.
28. Li Y, Xiong J, Guo W, Jin Y, Miao W, Wang C, Zhang H, Hu Y, Huang H. Decomposable black phosphorus nano-assembly for controlled delivery of cisplatin and inhibition of breast cancer metastasis. J Control Release. 2021;335:59–74.
29. Jin Y, Zhao B, Guo W, Li Y, Min J, Miao W. Penetration and photodynamic ablation of drug-resistant biofilm by cationic Iron oxide nanoparticles. J Control Release. 2022;348:911–23.
30. Jiang L, Li R, Xu J, Luan P, Cui Q, Pang Z, Wang J, Lin G, Zhang J. Endotoxin-adsorbing macrophage-mimetic hybrid liposome for sepsis treatment. Chem Eng J. 2019;371:15–25.
31. Li Y, Liu Y, Ren Y, Su L, Li A, An Y, Rotello V, Zhang Z, Wang Y, Liu Y, Liu S, Liu J, Laman JD, Shi L, Mei HC, Busscher HJ. Coating of a novel antimicrobial nanoparticle with a macrophage membrane for the selective entry into infected macrophages and killing of intracellular staphylococci. Adv Funct Mater. 2020;30:2004942.
32. Li Y, Wang M, Tao Y, Zhang R, Zhou M, Tao P, Feng PC, Huang W, Huang H, Miao W. Highly stable and biocompatible nanocontrast agent encapsulating a novel organic fluorescent dye for enhanced cellular imaging. Powder Technol. 2019;358:110–9.
33. Wang Y, Wang P, Cao HY, Ding HT, Su HN, Liu SC, Liu G, Zhang X, Li CY, Peng M, Li F, Li S, Chen Y, Chen XL, Zhang YZ. Structure of Vibrio collagenase VhaC provides insight into the mechanism of bacterial collagenolysis. Nat Commun. 2022;13:566.
34. Murphy EC, Frick IM. Gram-positive anaerobic cocci–commensals and opportunistic pathogens. FEMS Microbiol Rev. 2013;37:520–53.

Publisher's Note